QUAKES-I Annual Report 2023

Madeline Schwarz, J Ramon Arrowsmith
Arizona State University School of Earth and Space Exploration
November 8, 2023

Summary

Here we summarize the progress, findings, and next steps from the ASU team in our first year of support (September 2022-September 2023) for developing the airborne Quantifying Uncertainty and Kinematics of Earth Systems Imager (QUAKES-I) into an end-to-end operational system to meet the Surface Topography and Vegetation incubation program observables. These observables include the rapid response acquisition and analysis of sub-decameter resolution topography for analyses of earthquake, volcanic, and surface processes as well as furthering our understanding of the quality, limitations, and best-practices for stereo-imaging systems. The 2021 and 2022 flights collected ~480,000 and ~460,800 raw images respectively from the California plate boundary and portions of Arizona. We conducted preliminary photogrammetric processing of select 2022 QUAKES-I imagery from Death Valley and the San Andreas fault zone using Agisoft Metashape Professional Edition to generate and evaluate topographic products. These products include point clouds, digital elevation models (DEMs), and color ortho-mosaics. Results from our initial efforts include: 1) A functioning workflow for site-specific photogrammetric processing using Agisoft Metashape, 2) A draft workflow for an automated end-to-end processing pipeline, and 3) Identification of next steps for refining the processing workflow. These next steps include addressing discrepancies between the 2021 and 2022 data, evaluating the quality of topographic products in comparison to airborne laser scanning counterparts (EarthScope and USGS-3DEP), correcting systematic geolocation errors observed in the topographic products, and reducing data processing times.

Progress

Data Processing Pipeline Overview

The QUAKES-I data processing pipeline consists of four stages: data acquisition, photogrammetric processing, quality assessment, and scientific applications (Figure 1). The data acquisition stage refers to the collection of images in-flight by the QUAKES-I camera rig. Photogrammetric processing includes data pre-processing and SFM from which topographic products (point clouds, DEMs, and ortho-mosaics) are generated.

These products are evaluated for geolocation accuracy, topographic detail, and data resolution in the quality assessment stage. Once the data products are assessed and refined, they can be used to extract scientific information for a variety of solid earth applications.

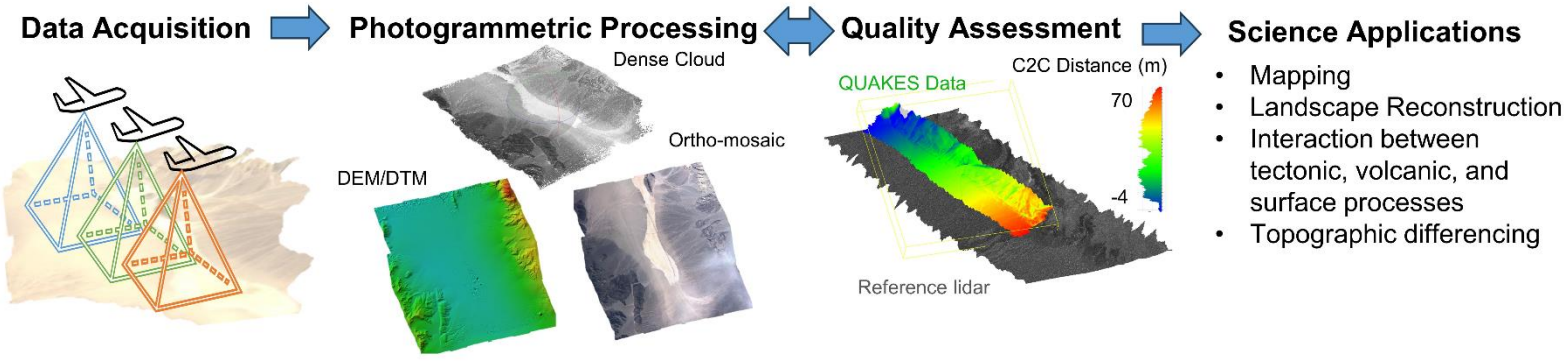

Figure 1. High-level outline of the QUAKES-I data processing pipeline. Processing consists of data acquisition with the 8-camera array on the Gulfstream V aircraft, photogrammetric processing with Python and Agisoft Metashape, quality assessment with Cloud Compare software, and the extraction of scientific information from topographic products.

Photogrammetric Processing Workflow

For the 2022 flight data, preliminary site-specific topographic products were generated using commercial photogrammetry software. These sites include Death Valley, the San Andreas Fault (SAF) creeping section, and Dragon's Back Ridge along the SAF in the Carrizo Plain, south central California (not presented here). We wrote python scripts leveraging open-source libraries to perform image pre-processing. To perform SFM, we utilized Agisoft Metashape Professional Edition 1.8.4 in parallel with the JPL team using Pix4D. Figure 2 summarize the workflow.

Data preparation

Images are processed in site-specific chunks of ~600-1,000 images to account for compute limitations and adequate image overlap during SfM alignment (Figure 2). Images from each of the eight cameras are demarcated by their file names, and the images' EXIF metadata contains the GPS coordinates of the cameras. We computed the euler angles (yaw, pitch, roll) for each of the eight cameras using the estimated camera extrinsics supplied in the camera-rig documentation for input into Metashape.

Photogrammetric Processing Pipeline

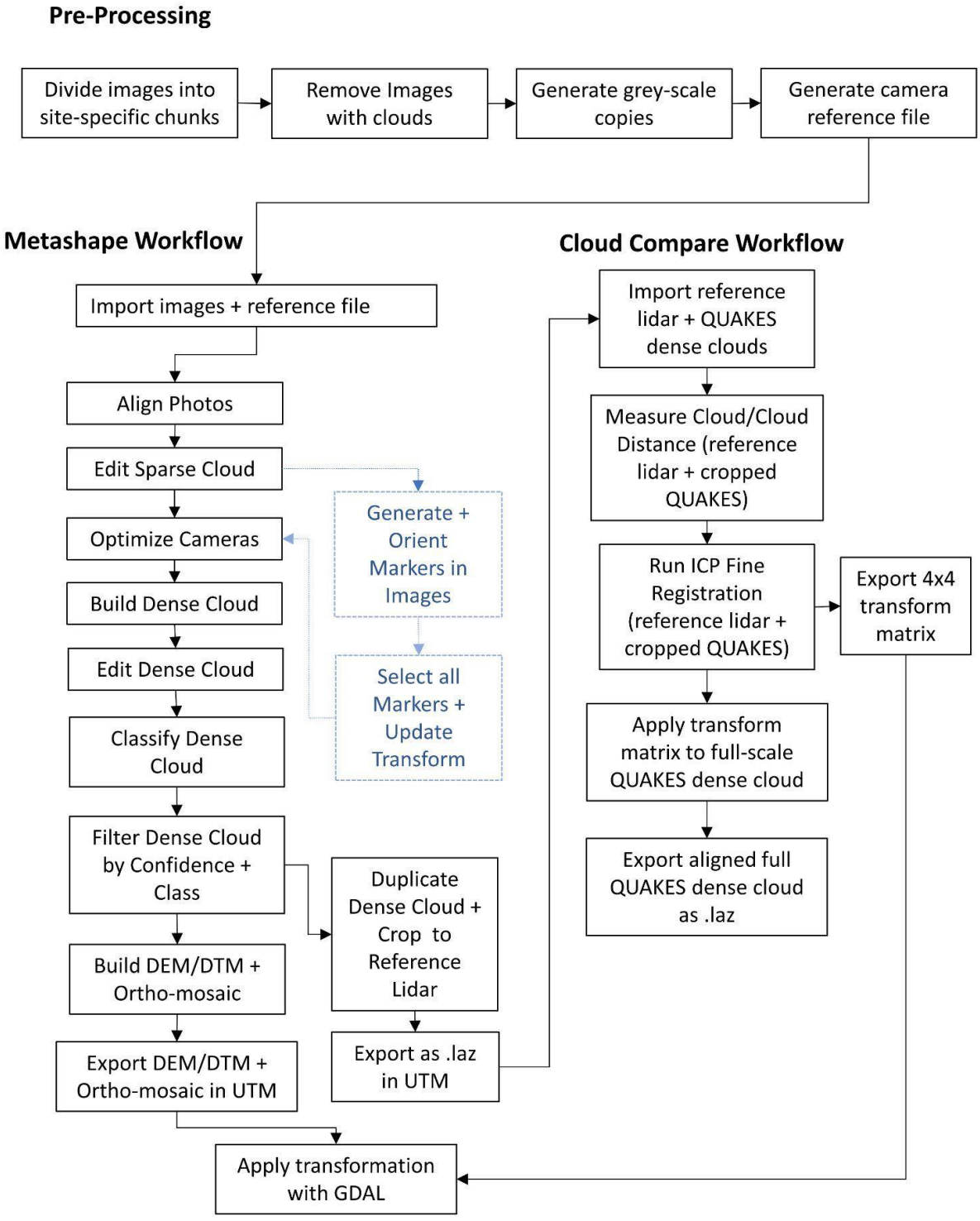

Figure 2. The full pipeline for the photogrammetric processing. Image pre-processing is accomplished using Python. Point clouds, DEMs, and ortho-mosaics are generated in Agisoft Metashape. Blue boxes in the Metashape workflow indicate the optional addition of ground control points in constructing the point cloud. ICP alignment is conducted in Cloud Compare.

In the image pre-processing stage, data for a given chunk is filtered by identifying and removing images containing clouds or excessive blurriness (Figure 2). Gray-scale copies of the adequate images are generated with the original metadata preserved. The purpose of applying a gray-scaling filter to the images is to enhance the number of tie points identified by the photogrammetry software during image alignment by minimizing errors introduced by color-variation between images. Next, a reference text file specifying camera GPS locations and orientations is written by extracting the camera IDs from each image filename and assigning the associated Euler angles and GPS coordinates to each image file.

SfM processing in Agisoft Metashape

The gray-scale images and the reference file are imported into Metashape as a single chunk. The SfM processing procedure in Metashape consists of image alignment to create a sparse cloud, then editing and optimizing it to generate a higher quality dense cloud. The dense cloud is classified and filtered to generate the DEM, DTM, and ortho-mosaic. Table 1 describes the specific Metashape tools and parameters used to process the imagery and create topographic products.

Metashape Tool/Procedure	**Parameter Name**	**Parameter Value**
Align Images	Accuracy	High
	Generic preselection	Yes
	Key point limit, Tie Point limit	40,000
	Exclude stationary tie points	Yes
Manual/Gradual Selection	*User selects and deletes erroneous points*	
Manual Ground Control Points (OPTIONAL)		
Place Markers	*User places markers in the Metashape basemap*	
Filter photos by marker	*User corrects the marker placement in each image*	
Update Transform	*Check all markers and select Update Transform button*	
Optimize Cameras	Parameters	f, b1, b2, cx, cy, k1-k4, p1, p2
	Fit additional corrections	Yes
Python Console *(re-map image paths back to color photographs)*	*chunk = Metashape.app.document.chunk* *new_path = r"" # path to color images*	

	for camera in chunk.cameras: *camera.photo.path = "/".join([new_path, camera.photo.path.rsplit("/",1)[1]])*	
Build Dense Cloud	Quality	High
	Filtering mode	Mild
	Point Confidence	Yes
	Point Color	Yes
Classify Points	Classes	Ground, High Vegetation
Filter Dense Cloud	Filter by Confidence	~2 or 3-255
	Filter by Class *(for DTM or DEM)*	Ground or Ground + High Vegetation
Build DEM	Coordinate system	WGS 84 (EPSG::4326)
	Source data	Dense cloud
	Interpolation	Enabled
Build Ortho-mosaic	Coordinate system	WGS 84 (EPSG::4326)
	Colors	3 bands, uint8
	Blending mode	Mosaic
	Surface	DEM
	Enable hole filling	Yes

Table 1. Summary of the tools and parameters used in Agisoft Metashape Professional Edition 1.8.4.

Geolocation correction using Ground Control Points (GCPs)

For aerial surveys, a level of uncertainty is always present in the aircraft positioning and pointing which results in geolocation errors in the 3D reconstructions of topography. A common method for correcting geolocation error is the use of manually placed ground control points (GCPs) that snap the model to the proper orientation and position of the land surface. We generate GCPs with the Metashape basemap by marking and sampling points within the data chunk area through the Model viewer pane. The Metashape basemap imagery is Sentinel-2 Cloudless (EOX IT, 2021). A minimum of 5-7 GCPs is required to properly correct the model, and more GCPs are recommended due to the size of the processing chunks. GCPs are evenly spaced throughout the study area, and placed in relatively flat, recognizable locations such as roads or preserved geologic features. The GCPs are added as ‘markers’ using the ‘Place Marker’ tool or by importing a table of GCPs into the Metashape Reference pane. Next, the markers are identified and corrected in each image using the ‘filter photos by marker’ tool and manually editing marker placement in the photographs. Once the markers are correctly placed in the images, all of the markers are selected in the Reference pane and the ‘Update Transform’ tool is applied. This reorients the sparse cloud and dense cloud with respect to the control points (Figure 2).

Geolocation correction using ICP alignment

Another method for correcting geolocation error is iterative closest point (ICP) alignment (Figure 2). We correct geolocation errors in the QUAKES-I dense clouds by performing ICP alignment in Cloud Compare with overlapping 0.5-1m EarthScope and USGS 3DEP lidar datasets available from OpenTopography. These data are high resolution, accurately geolocated, and overlap consistently with most of the 2022 QUAKES-I flight path. We use ICP alignment both as an alternative to manually placed GCPs and in tandem to control points depending on the initial dense cloud quality.

To perform ICP alignment, we first export the filtered dense cloud from Metashape as an .laz file projected into the local WGS84 UTM coordinates. We then extract the extent of the dense cloud and perform a data search on OpenTopography to find an overlapping EarthScope or 3DEP point cloud (~2-3x3km sized swath). In Metashape, we generate a duplicate of the QUAKES-I dense cloud and crop the duplicate cloud to fit within the extent of the reference point cloud. The cropped duplicate dense cloud is then exported as an .laz file projected into the same local WGS84 UTM coordinates.

Next, the reference point cloud, the cropped QUAKES-I dense cloud, and the full QUAKES-I dense cloud are imported into Cloud Compare without applying any global shifts to the data (Figure 2). We first measure the cloud-to-cloud distance between the reference data and the cropped QUAKES-I data using the Cloud-to-cloud distance tool with the ‘separate x,y,z distances’ parameter checked. Next, we perform ICP alignment using the ‘ICP fine registration’ tool. We set the cropped QUAKES-I .laz as the ‘aligned’ input parameter and the lidar .laz as the ‘reference’ input parameter. The RMSE parameter is checked and set to 1×10^{-3} meters. Upon completion, the cropped QUAKES-I dense cloud will be aligned to the lidar reference point cloud and Cloud Compare will generate the resulting transform as a 4x4 matrix. We then apply this transform to the full QUAKES-I dense cloud using the ‘Apply Transform’ tool. The aligned full QUAKES-I dense cloud is saved as a new .laz file and can be re-imported into Metashape.

DEM, DTM, and Ortho-mosaic

Once the dense cloud is generated, geolocated, and filtered, it is used to produce the DEM, DTM, and ortho-mosaic (Figure 2). We build DEMs by filtering the dense cloud by class (ground) and running the ‘Build DEM’ tool with the source set to ‘Dense Cloud’. The ortho-mosaic is generated with the ‘Build Ortho-mosaic’. Both topographic products can be exported from Metashape as .tif files in the desired coordinate system.

Data Quality Assessment

We evaluate the quality of QUAKES-I topographic products in comparison to EarthScope and USGS 3DEP lidar-derived point clouds and DEMs using 3D cloud-to-cloud distance measurements in Cloud Compare (Figure 2).

Results

Here we present initial results from our photogrammetric workflow using Agisoft Metashape for the Panamint Valley in Death Valley and the San Andreas Fault creeping section.

Panamint Valley, Death Valley California

The area imaged in flight Line 1 across Death Valley in 2022 is a ~15 by 15 km swath covering the Panamint Valley in California (Figure 3). This valley is bounded on its eastern side by mountains of the Panamint Range and the Argus Mountains to the west. The valley consists of a relatively flat dry lakebed in the center with sloping alluvial fans along the bounding range fronts and volcanic deposits from a Pliocene cinder cone to the southwest. Along the eastern range front, the Panamint fault zone crosscuts multiple alluvial fan surfaces and offsets multiple river channels. Along the western bounds of the valley, the Ash Hill fault crosscuts both alluvial fan surfaces and volcanic units (Jayko, 2009).

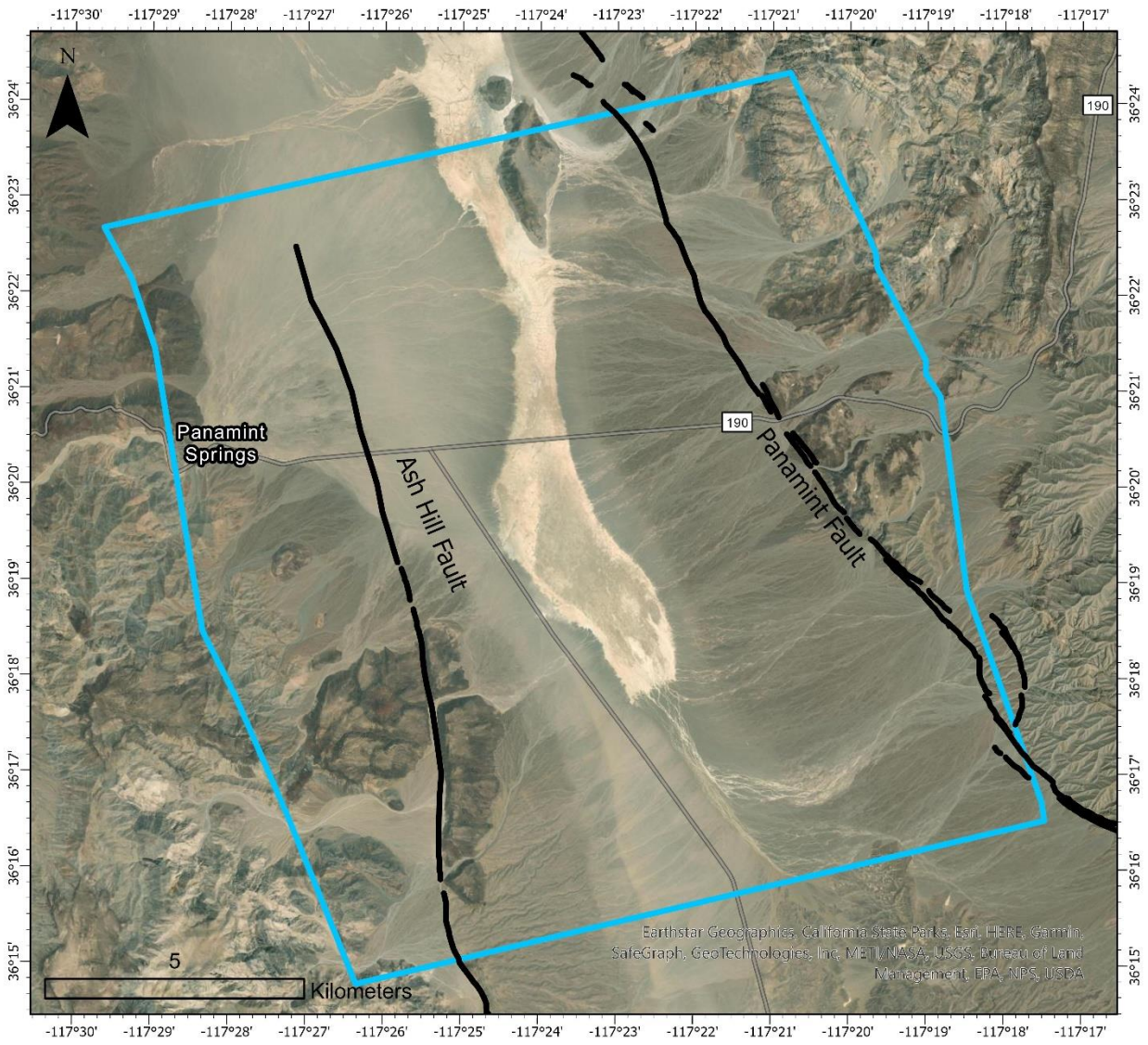

Figure 3. Map of Panamint Valley coverage by the 2022 QUAKES-I flight line over Death Valley. The blue box indicates the extent of QUAKES-I coverage and the black lines represent the Ash Hill and Panamint faults (Jayko, 2009).

QUAKES-I collected 1,760 images for the Panamint Valley swath of which 681 contained no clouds and thus had clear view of the land surface. We processed these images using the workflow outlined in Figure 2. Camera position and extrinsic information adequately reconstructed the land surface topography during alignment to form a single point cloud model. However, the resulting dense cloud from camera reference information alone exhibited significant horizontal geolocation error in which the dense cloud was offset ~380 meters northeast of the flight path. The dense cloud also exhibited warping at the edges of the model <20 meters in amplitude. A total of 14 ground control points (Figure 4) created with the Metashape base map were utilized to

reduce these errors prior to further geolocation correction with ICP alignment. We classified the dense cloud into ground points and high vegetation points and built the DTM from the dense cloud (Figure 5A). The resulting DTM resolution is 1.61 meters per pixel.

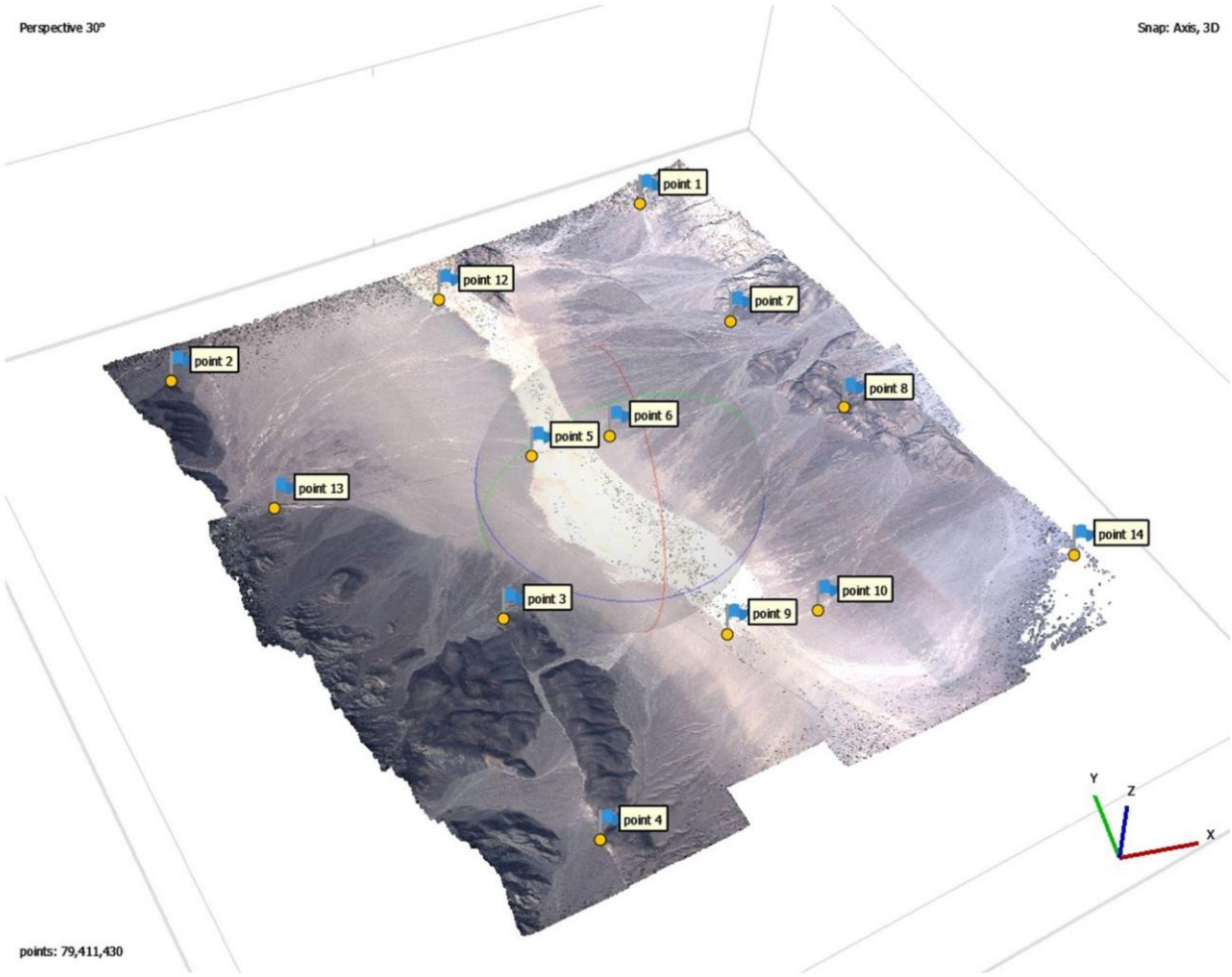

Figure 4. Oblique view of the Panamint Valley (Figure 3) dense cloud generated in Agisoft Metashape. Dense cloud colors are those of the original QUAKES-I images. The dense cloud consists of 79,411,430 points. Yellow points indicate ground control points used to perform initial geolocation correction.

Qualitatively, the DTM accurately visualizes topography– topographic highs of the two bounding range fronts, alluvial fan surfaces, fault scarps, and channels are clearly visible in the DTM. Artifacts in the DTM are present predominantly around the edges exhibiting excessive roughness and smoothness that is uncharacteristic of the natural

topography. Some rough artifacts are also visible within the dry lakebed at the center of the model (Figure 5A).

We generated a color ortho-mosaic of the Panamint Valley from the DTM and the QUAKES-I images (Figure 5B). The ortho-mosaic exhibits a linear artifact of shadowy bumps along the center of the model that corresponds to the flight path and thus may be shadows from the Gulfstream V aircraft. The southeastern portion of the mosaic exhibits white discoloration from partial cloud cover in the images used to reconstruct the model. Although the cloud filtering script initially removed these photos, we included them so that the DTM would capture the full extent of the Panamint fault segments crosscutting the quaternary fan deposits within the swath. From the color ortho-mosaic, the surficial geological units of the dry lakebed, alluvial fans, and basalt flows can be identified and distinguished.

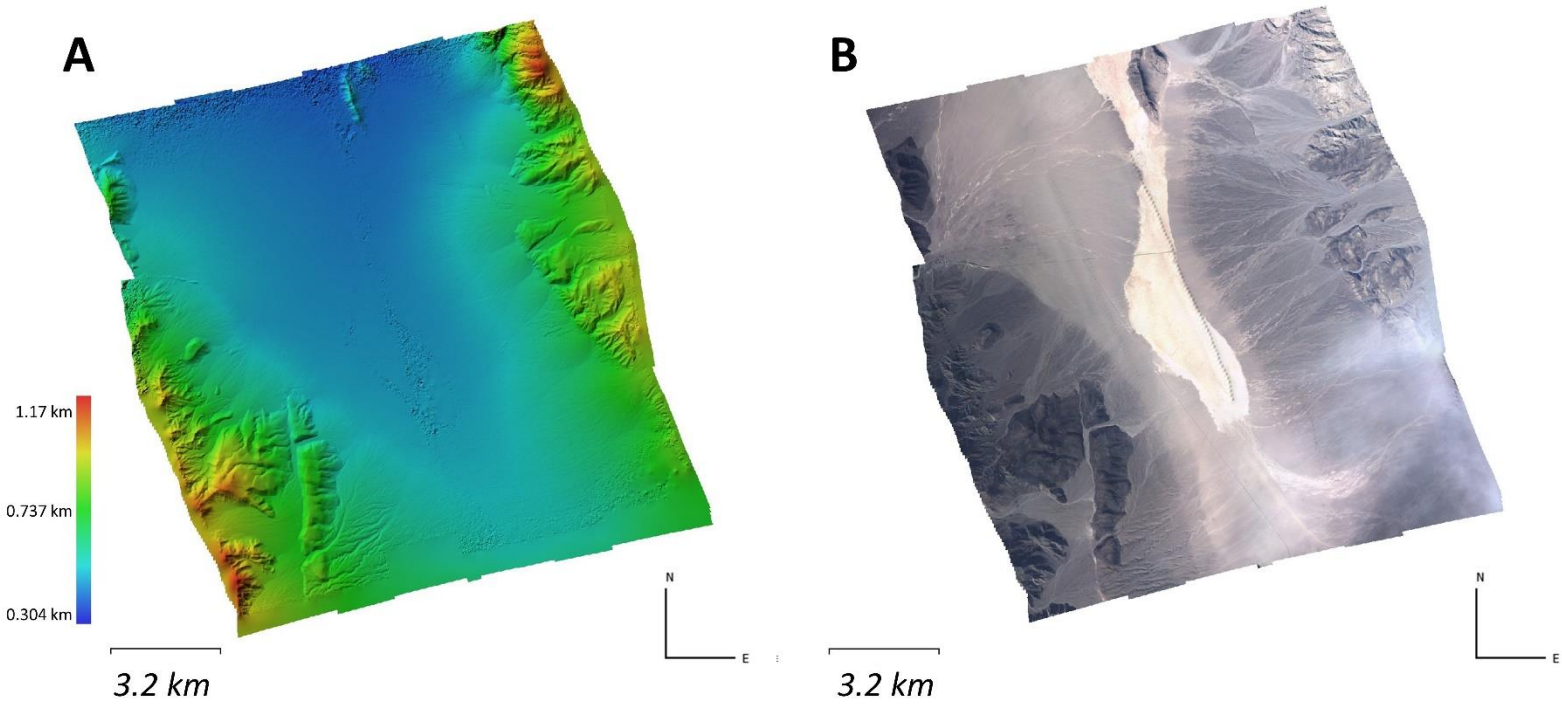

Figure 5. DTM (A) and color ortho-mosaic (B) of the Panamint Valley.

We conducted geolocation correction and data quality assessment for the QUAKES-I dense cloud with EarthScope lidar data (EarthScope Southern & Eastern California Lidar Project, 2009). The lidar data has a point density of 4.61 points/m^2 and raster resolution of 0.5 meters. The EarthScope lidar consisted of points for ground and high vegetation. that overlaps with the southeastern section of the QUAKES-I swath containing the Panamint fault (Figure 6A). Cloud-to-cloud distances for X, Y, and Z

comparing the QUAKES-I dense to the reference EarthScope lidar directions are shown in Figure 6. The positive and negative signs on the distance values reflect the point offset direction relative to the origin of the respective axis (X, Y, or Z).

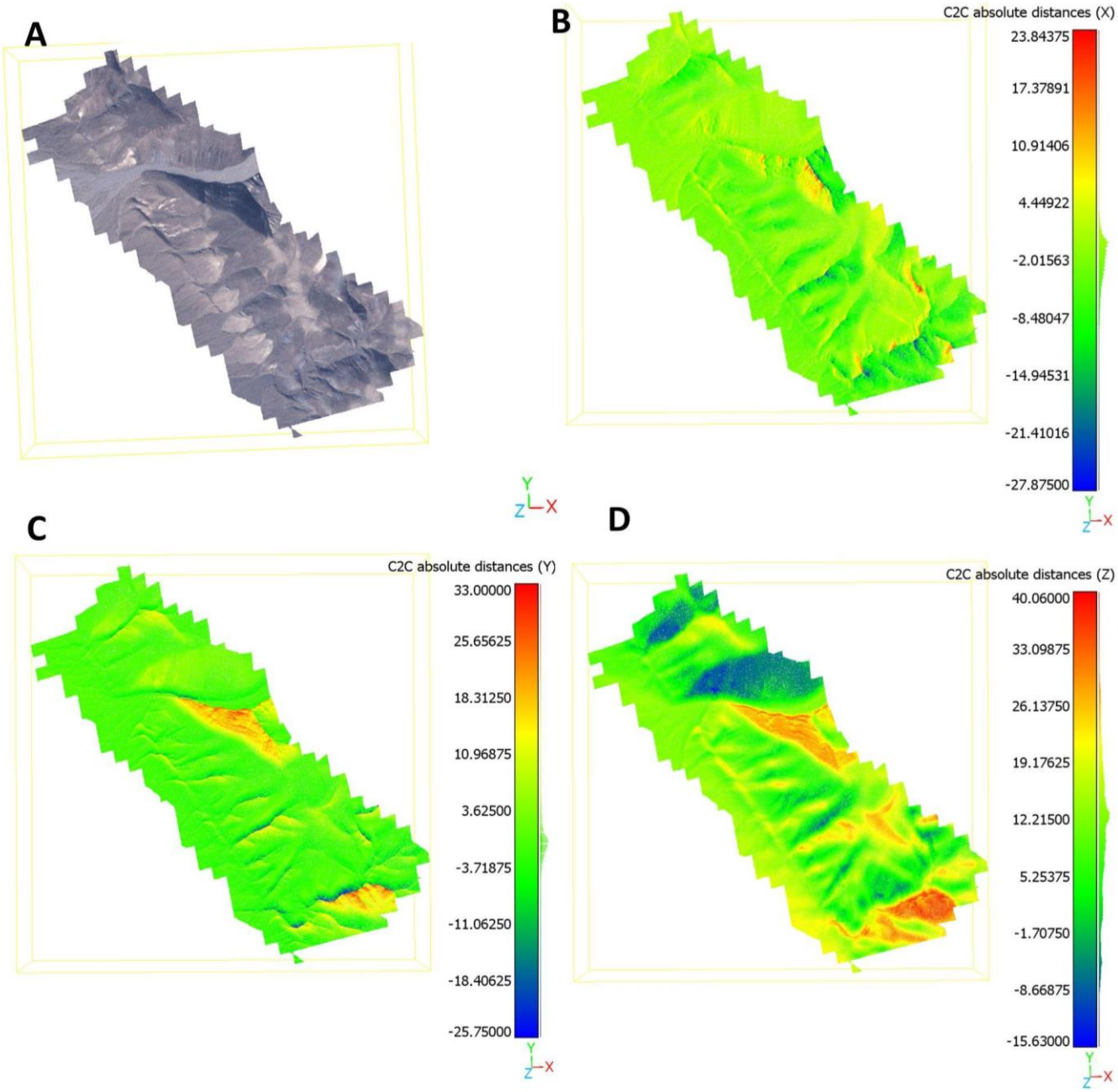

Figure 6. Cloud-to-Cloud distances <u>prior to ICP alignment</u> comparing the QUAKES-I dense cloud for Panamint Fault, Death Valley to reference EarthScope lidar. Distances displayed are in meters and histograms along the color scale reflect pixel abundance per distance value. A) The true-color QUAKES-I dense cloud (cropped) generated with 14 GCPs; B) The horizontal X distance between the QUAKES-I dense cloud and the reference point cloud; C) The horizontal Y distance between the QUAKES-I dense cloud

and the reference point cloud; D) The vertical Z distance between the QUAKES-I dense cloud and the reference point cloud.

For X distances, the QUAKES-I dense cloud shows an offset range of -28 meters to 24 meters with most points falling within -8.5 to 4.5 meters of the EarthScope point cloud (Figure 6B). For Y distances, the QUAKES-I dense cloud shows an offset range of -26 meters to 33 meters with most points falling within -3.7 to 3.7 meters of the EarthScope point cloud (Figure 6C). For the Z direction, the QUAKES-I dense cloud shows an offset range of -28 to 41 meters with most points falling within 5.0 to 19 meters of the EarthScope reference point cloud (Figure 6D). These distance measurements indicate that the QUAKES-I dense cloud is offset horizontally ~30 meters north of the EarthScope reference lidar data. Thus, adding the 14 GCPs to the dense cloud reduced the horizontal geolocation error from ~380 meters offset to ~30 meters offset.

To correct further correct the model's geolocation error, we performed ICP alignment using the 'Fine ICP Registration' tool. The transform matrix generated from ICP is applied to the DTM and ortho-mosaic (Figure 2). We then assess the quality of the registered QUAKES-I point cloud by re-measuring the X, Y, and Z cloud-to-cloud distances from the reference EarthScope point cloud. Figure 7 shows the resulting measurements. Post-ICP alignment, X offsets reduced to a range of -3.9 to 4.4 meters with most points showing distances between approximately -0.8 to 0.2 meters (Figure 7B). Y offsets reduced to a range of -4.0 to 5.3 meters with most points falling between -0.5 to 0.6 meters (Figure 7C). Z offsets which represent differences in elevation between the two point clouds are reduced to a range of -4.1 to 5 meters. Most of the points exhibit Z distances between -0.8 to 0.5 meters (Figure 7D). Points showing offsets outside of the majority-range distances are found where slopes in the topography are steep and where shadows are present in the QUAKES-I images. These results show that manually placed GCPs and ICP alignment with the EarthScope lidar-derived point cloud corrected the QUAKES-I dense cloud to <5-meter accuracy. The total end-to-end processing time for the Panamint Valley model is 5 hours and 2 minutes. This processing time includes image pre-processing, SfM in Metashape (including the manual placement of GCPs), and geolocation correction/quality assessment in Cloud Compare.

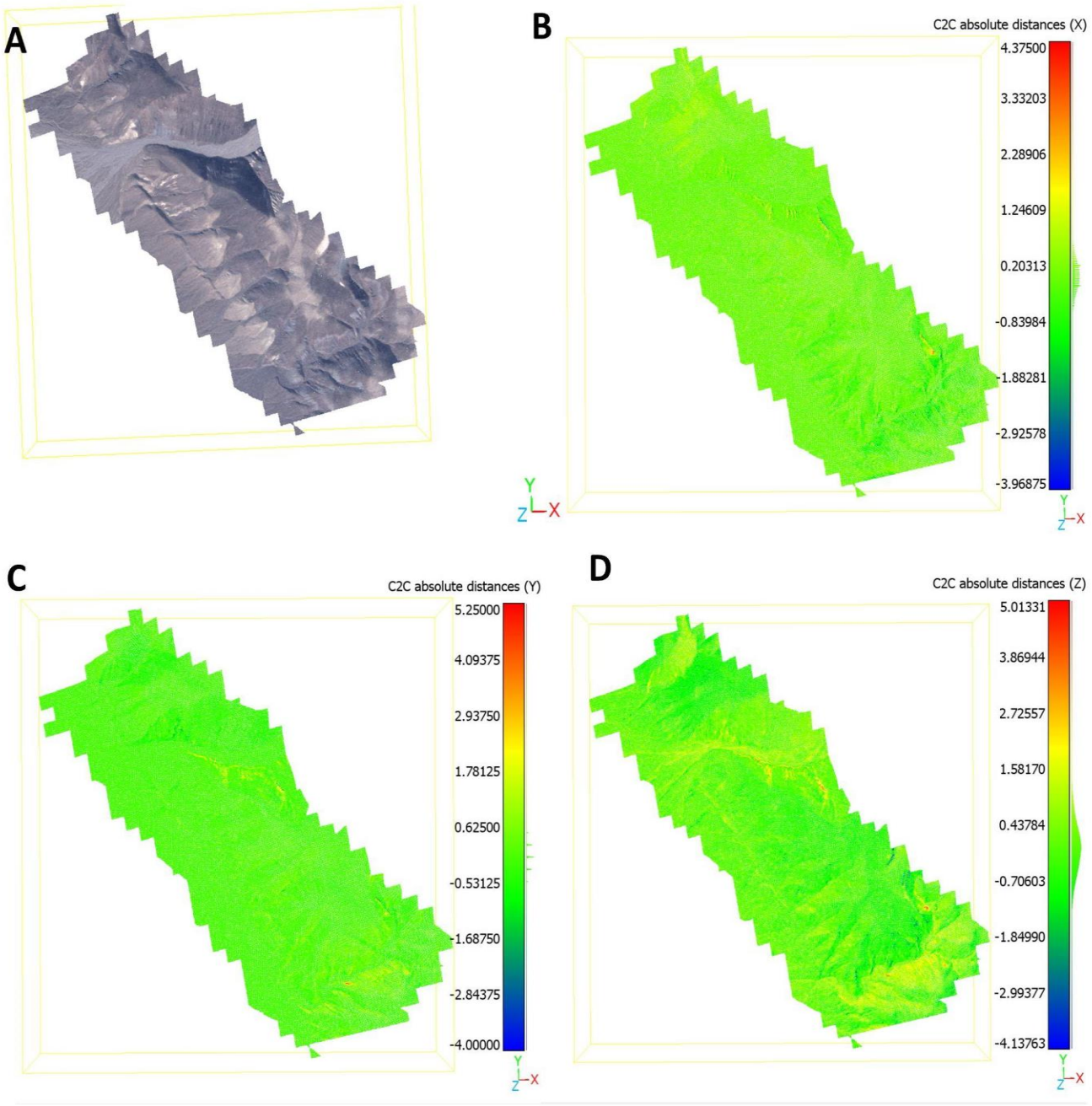

Figure 7. Cloud-to-Cloud distances after performing ICP alignment to register the QUAKES-I dense cloud for Panamint Fault, Death Valley to reference EarthScope Lidar. Distances displayed are in meters and histograms along the color scale reflect pixel abundance per distance value. A) The true-color QUAKES-I dense cloud (cropped) generated with 14 GCPs and aligned to the reference lidar using the ICP Fine Registration tool in Cloud Compare; B) The horizontal X distance between the QUAKES-I dense cloud and the reference point cloud; C) The horizontal Y distance between the QUAKES-I dense cloud and the reference point cloud; D) The vertical Z distance between the QUAKES-I dense cloud and the reference point cloud.

San Andreas Fault, Creeping Section

The area imaged in flight line 6 along the San Andreas Fault creeping section (CSAF Line 6) in 2022 is a ~15 by 23-kilometer swath centered on the San Andreas fault extending north from Dry Lake Valley and northeast of Pinnacles National Park (Figure 8). The swath also includes portions of the Calaveras fault, the San Benito fault, and the Pine Rock fault. The topography of the area consists of rugged mountains interspersed with lower laying hills and meandering river valleys.

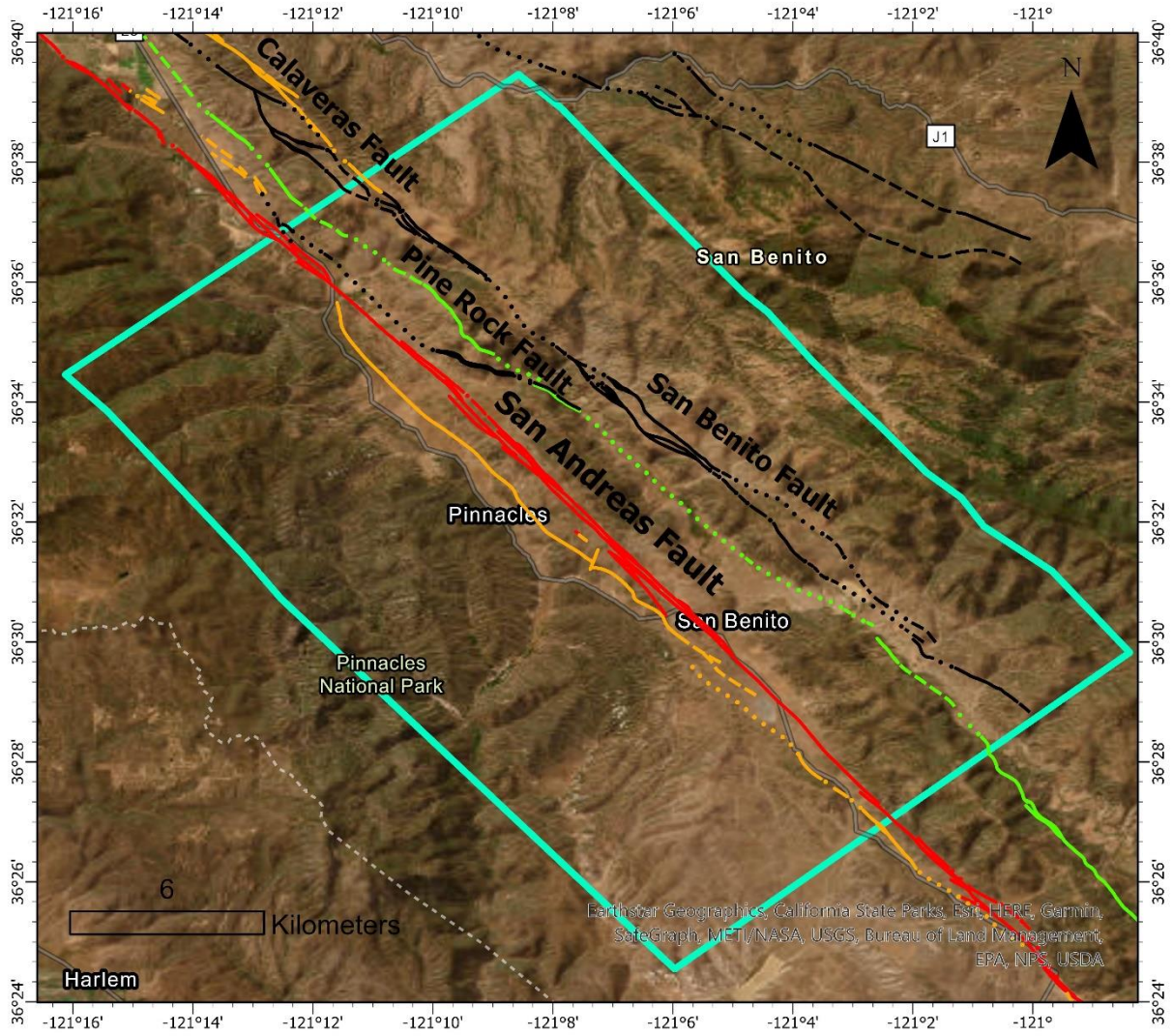

Figure 8. Map showing QUAKES-I coverage of the San Andreas fault Creeping section north of Dry Lake Valley. The blue rectangle represents the coverage area. Lines represent faults mapped in the USGS Quaternary faults database and are colored based on time of most recent surface deformation. Red represents historical (<150 years), orange is latest quaternary (<15,000 years), green is late quaternary (<130,000

years) and black is undifferentiated quaternary (<1.6 million years). Fault names are indicated in black text above their associated fault lines (U.S. Geological Survey, 2020).

QUAKES-I collected 962 images for the CSAF Line 6 swath. We processed these images using the workflow outlined in Figure 2. Camera position and extrinsic information properly reconstructed the land surface topography during alignment and generated a single point cloud model. The resulting dense cloud from camera reference information alone exhibited horizontal geolocation error but did not show any warping or roll in the model reconstruction. For this reason, we did not add GCPs to the dense cloud in addition to performing ICP alignment. We classified the dense cloud into ground and high vegetation classes and built the DTM from the dense cloud (Figure 10A). The resulting DTM resolution is 1.56 meters per pixel.

The DTM accurately visualizes the vegetation and topography of the land surface and exhibits only smooth artifacts around the model edges. We built the color ortho-mosaic from the DTM and QUAKES-I images (Figure 10B). The ortho-mosaic for this swath also contains artifacts that appear as linear bumps along the flight-line path like those observed in the Panamint Valley ortho-mosaic.

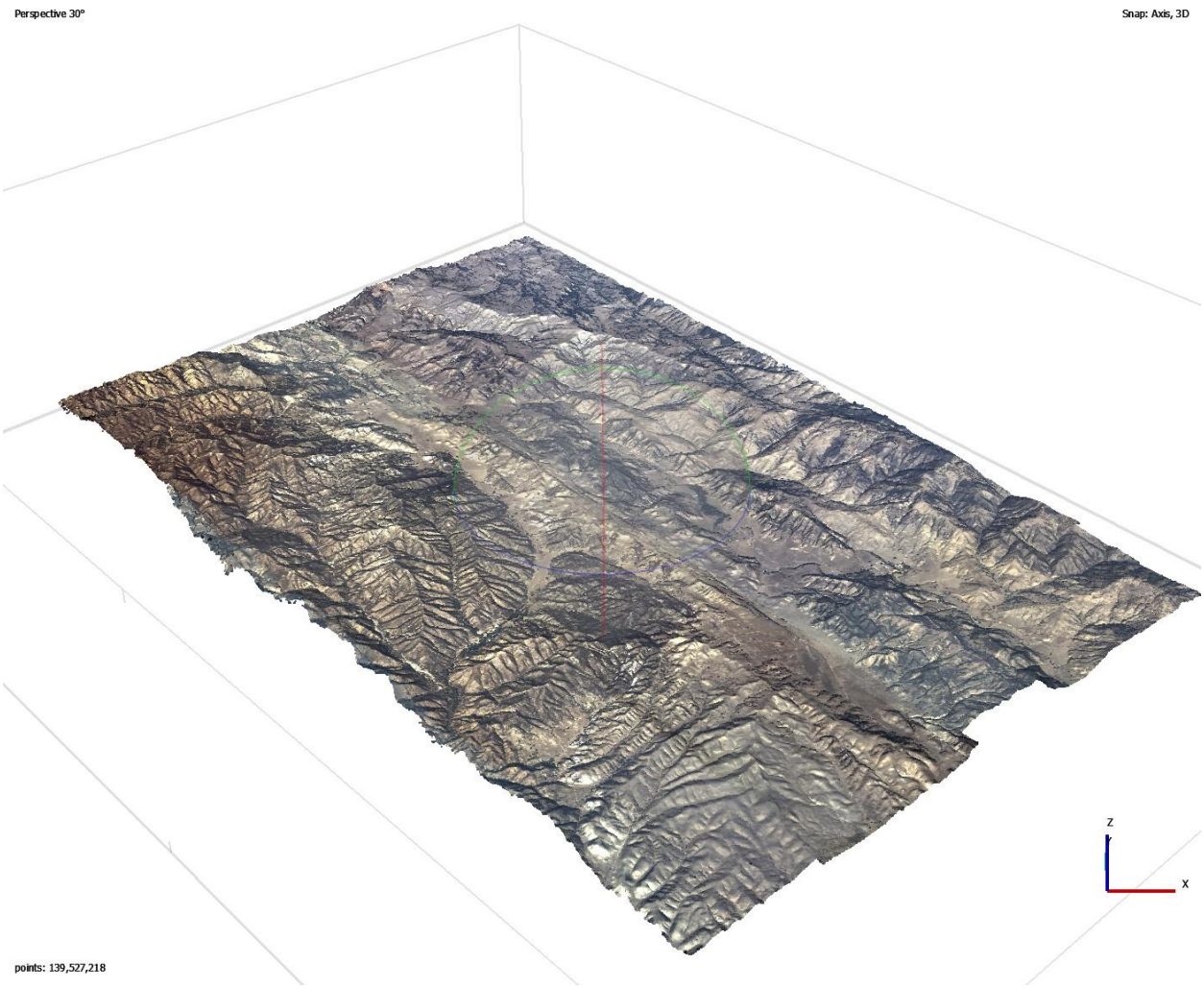

Figure 9. Oblique view of the CSAF Line 6 dense cloud generated in Agisoft Metashape. Dense cloud colors are that of the original QUAKES-I images. The dense cloud consists of 139,527,218 points.

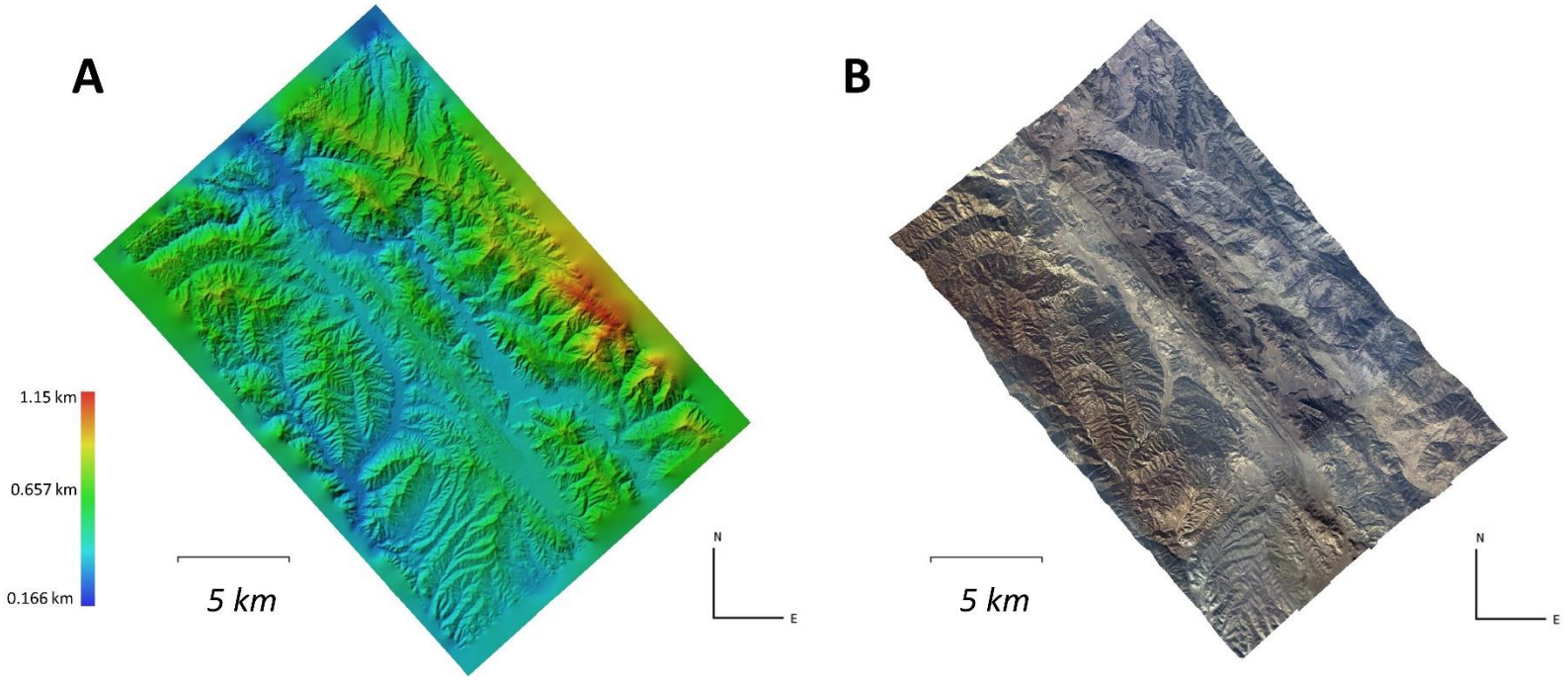

Figure 10. DTM and color ortho-mosaic of the San Andreas Fault creeping section.

We performed geolocation correction on the dense cloud with ICP alignment. For the reference dataset, we used USGS 3DEP lidar from the CA FEMA survey (U.S. Geological Survey, 2018). The lidar is classified for ground and high vegetation points, has a point density of 5.7 points/square-meter, and a 1-meter raster resolution. Figure 11 shows the X, Y, and Z cloud-to-cloud distances of the QUAKES-I creeping section point cloud to the reference point cloud prior to ICP registration. X distances range from -82 to 85 meters with most points showing distances around 1.7 meters. Y distances range from -64 to 85 meters with most points falling between 8.0 and 10 meters. Z distances range from -111 to 147 meters with a relatively even spread between -50 and 17 meters. These distance measurements show that the QUAKES-I point cloud is offset horizontally ~380 meters to the northeast from the reference point cloud.

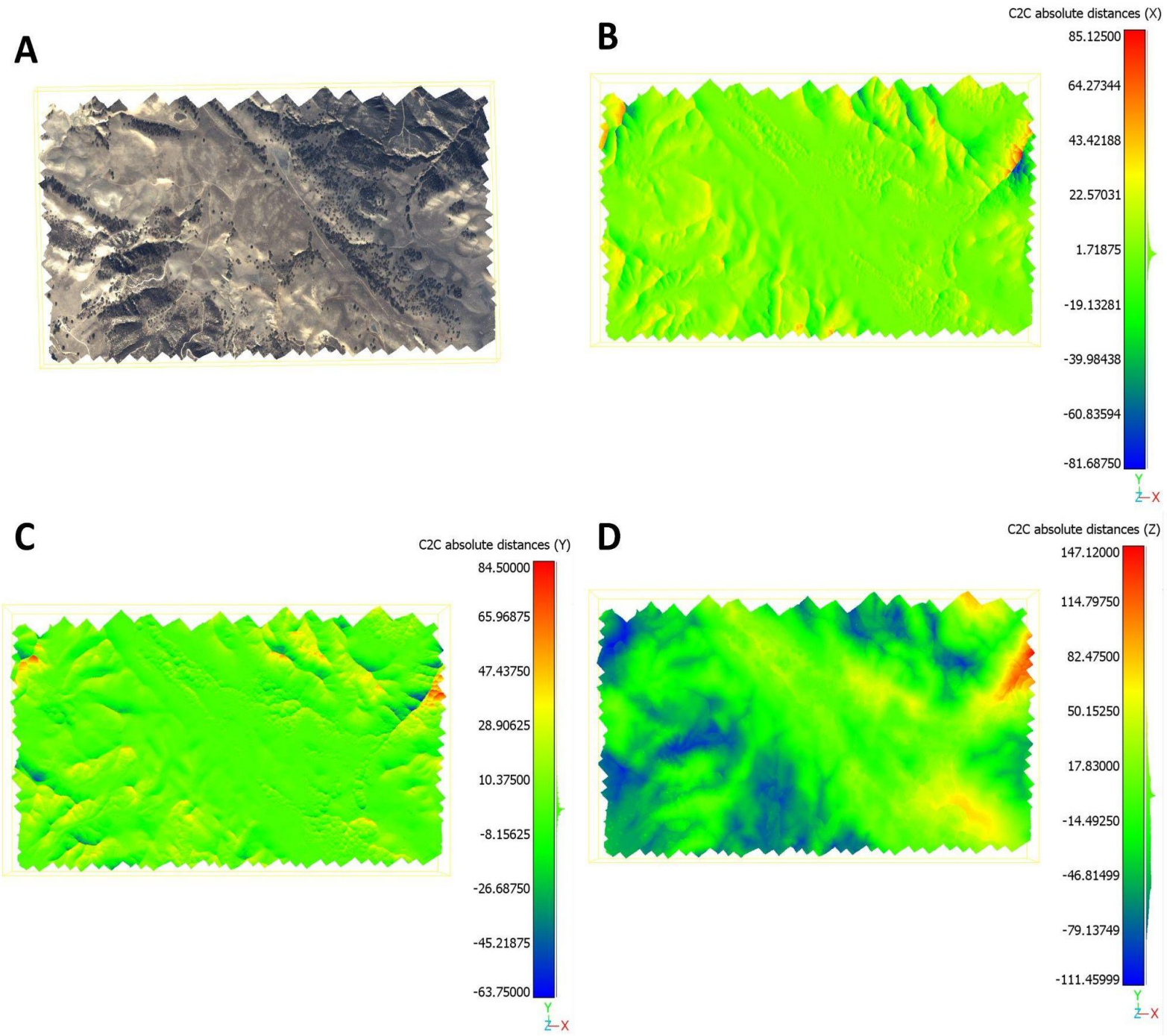

Figure 11. Cloud-to-Cloud distances prior to ICP alignment comparing the QUAKES-I dense cloud for the CSAF Line 6 section to reference 3DEP lidar. Distances displayed are in meters and histograms along the color scale reflect pixel abundance per distance value. A) The true-color QUAKES-I dense cloud (cropped); B) The horizontal X distance between the QUAKES-I dense cloud and the reference point cloud; C) The horizontal Y distance between the QUAKES-I dense cloud and the reference point cloud; D) The vertical Z distance between the QUAKES-I dense cloud and the reference point cloud.

To correct this large horizontal geolocation error, we performed ICP alignment and remeasured the cloud-to-cloud distances (Figure 12). From ICP alignment, offsets in the X direction reduced to a range of -9.12 to 8.87 meters with most points showing distances around -0.12 meters. Y offsets reduced to a range of -8.00 to 6.00 meters with most points falling between -1.00 and 0.75 meters. Z offsets show a range of -40.21 to 7.00 meters with most points falling between -2.00 and -1.10 meters. Similar to the Panamint Valley dense cloud, points with offset distances that fall outside the majority range are located on steep topographic slopes and where shadows are present in the QUAKES-I images. From these measurements, we conclude that after ICP alignment, the QUAKES-I dense cloud is <8-meter accuracy of the reference point cloud. The total end-to-end processing time for the CSAF Line 6 is 6 hours and 3 minutes. This processing time includes image pre-processing, SfM in Metashape, and geolocation correction/quality assessment in Cloud Compare.

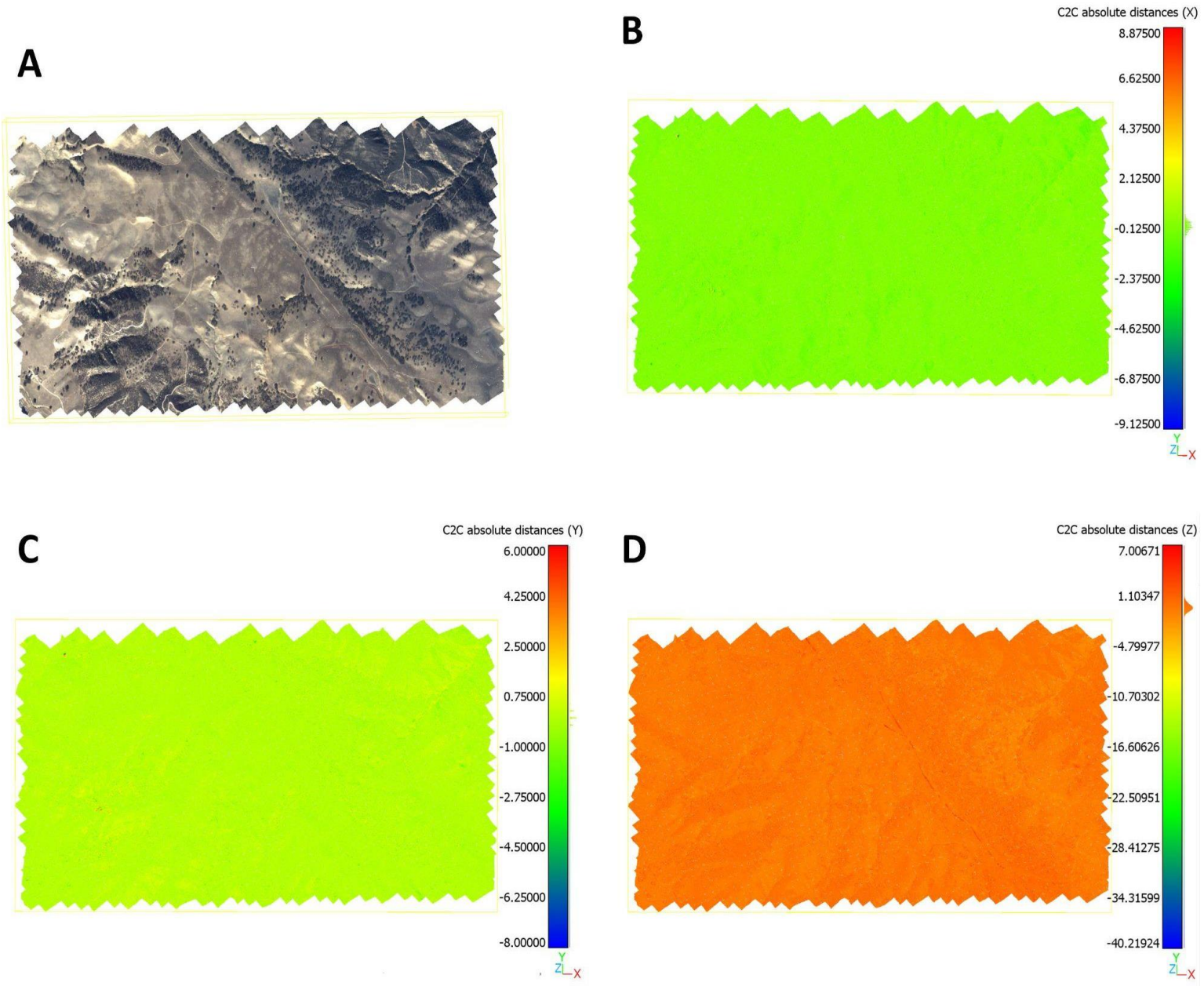

Figure 12. Cloud-to-Cloud distances <u>after performing ICP alignment</u> to register the QUAKES-I dense cloud for the CSAF Line 6 section to reference 3DEP lidar. Distances displayed are in meters and histograms along the color scale reflect pixel abundance per distance value. A) The true-color QUAKES-I dense cloud (cropped); B) The horizontal X distance between the QUAKES-I dense cloud and the reference point cloud; C) The horizontal Y distance between the QUAKES-I dense cloud and the reference point cloud; D) The vertical Z distance between the QUAKES-I dense cloud and the reference point cloud.

Discussion

Metashape workflow and pre-processing procedures

We developed our photogrammetric processing pipeline through adaptation of standard SfM procedures and through experimentation with QUAKES-I imagery (Agisoft LLC., 2022; Betlem, et al., 2022; Johnson, et al., 2014). Initial alignment experiments from the software's estimation of camera positions/angles (without any GCPs) yielded duplicate point clouds with excessive roll/tilt as shown in Figure 13. This prompted us to recompute the camera extrinsics from the QUAKES-I rig rotation matrices and write the script automating the generation of camera reference files for input into Metashape. The addition of camera extrinsics solved the 3D reconstruction issue for most data chunks. It is worth noting that by default, Metashape treats each image as its own separate 'camera' unless the user divides the images into 'Camera Groups' with a specified 'Camera Model.' Through experimentation, we found that specifying camera groups and inputting camera model parameters had no effect on the quality of alignment and sparse cloud generation. This was the case both before and after inputting camera extrinsics into the images' reference. Thus, we opted to use the default setting in which each image is treated as an independent camera in the alignment process. We conclude that the single-line flight path combined with the complexity of an 8-camera array is likely the source of issues in 3D reconstruction, and therefore it is necessary to include camera position and angle information to constrain image alignment. We also included the grey-scale image conversion step in our pre-processing procedure to increase the number of automatic tie points identified by Metashape in the alignment stage. This step was utilized by the JPL group in processing images from the 2021 QUAKES-I flight.

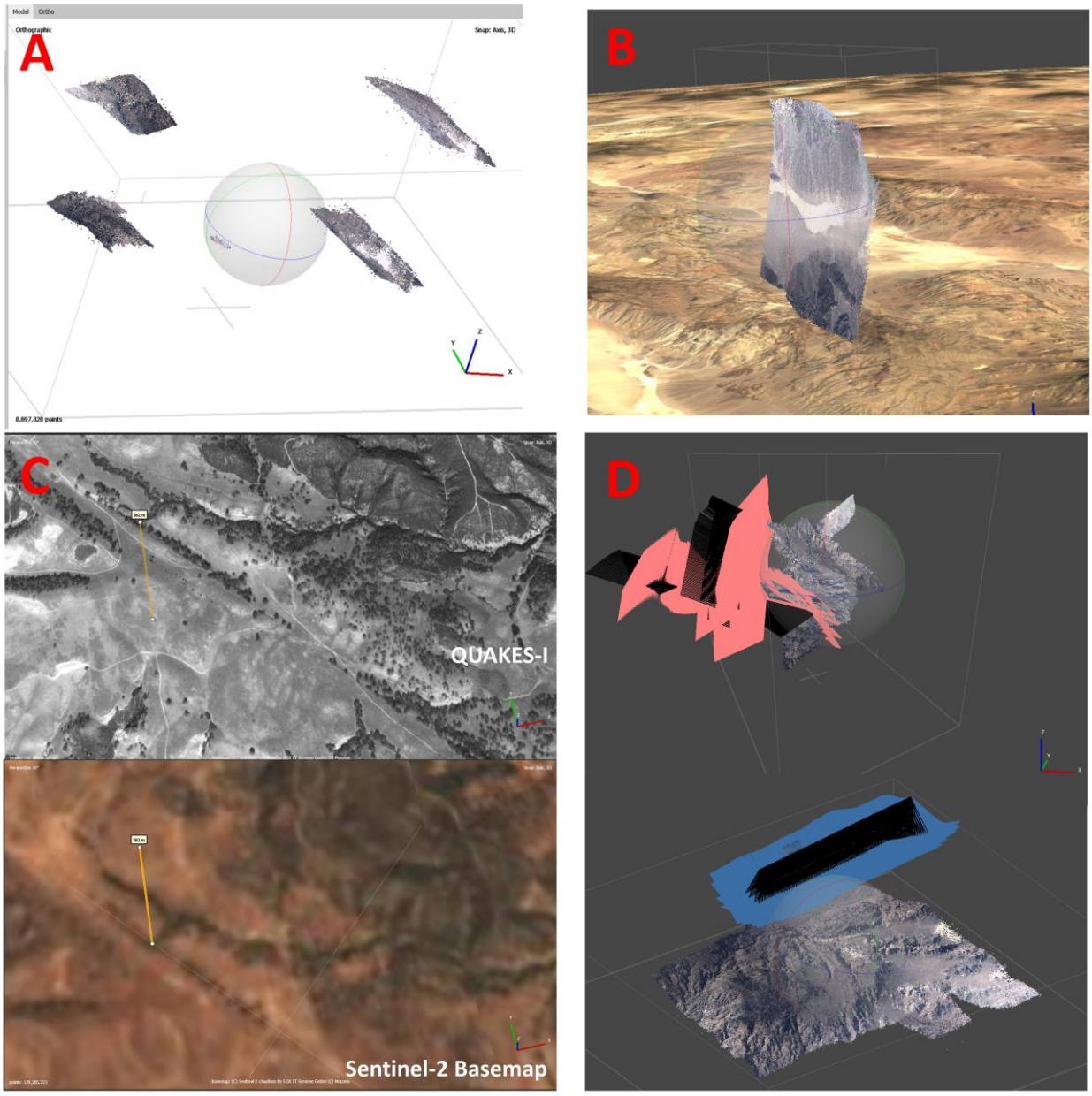

Figure 13. Examples of point cloud errors in Metashape prior to refining pre-processing procedures. A) Sparse clouds for Death Valley lines 5 (left) and 1 (right) exhibiting duplicate planes and excessive tilt due to missing camera position and orientation values. B) Dense cloud for the Panamint Valley showing a single plane, but near-90 degree tilt due to missing camera orientation values. C) Visualization of the systematic ~380 meter horizontal offset present in QUAKES-I topographic products prior to geolocation correction with GCPs or ICP alignment. D) Visualization of different sparse cloud results using 'Reference Selection' (upper) vs 'Generic Pre-selection' (lower) parameters during Metashape alignment.

Geolocation correction

QUAKES-I topographic products generated in Metashape from camera position and orientation information alone consistently exhibit horizontal geolocation error in which the model is shifted horizontally ~380 meters approximately 20-30 degrees from the direction of flight path (Figure 13C). Initial results from processing Panamint Valley and CSAF Line 6 demonstrate that QUAKES-I camera position and extrinsic information alone is not sufficient to produce accurately geolocated topographic products. Without ground control points, the 3D reconstruction of Panamint Valley showed the ~380 meters offset northeast of the flight path as well as warping at the edges of the point cloud. In comparison, the CSAF Line 6 model showed the same ~380-meter horizontal offset however did not show any model warping which may be attributed to the difference in topography within the swaths (i.e. low central topography bounded by high topography at model edges in the case of Panamint Valley).

GCPs added to the Panamint Valley model partially corrected the horizontal geolocation error reducing it from ~380 meters to ~30 meters. The GCPs also corrected the warped model edges, making it feasible to properly conduct ICP alignment and apply the resulting transform to the entire dense cloud. The 14 GCPs used in the Panamint Valley model were created within Metashape by sampling the Sentinel-2 base map which has an accuracy of ~20 meters (Claverie, et al., 2018). GCPs sourced from higher resolution datasets may do a better job of reducing geolocation error.

The addition of GCPs to the model adds approximately 0.5-1 hour to the overall processing time depending on the number of GCPs placed, topographic complexity of the study area, and experience of the user with Metashape software. This is because GCPs must be *manually placed* and corrected in each image containing the placement location.

ICP alignment results for the Panamint Valley model demonstrate that the combination of manual GCPs and ICP registration with a high-quality reference dataset can correct QUAKES-I product geolocation accuracy to <5 meters. ICP alignment results for the CSAF Line 6 show that for certain datasets, camera position and extrinsic information paired with ICP alignment can correct significant geolocation errors up to <8-meter accuracy, and the addition of manual GCPs can be skipped. However, this can only be applicable if the 3D reconstruction produces a dense cloud without warping or roll. Otherwise, ICP alignment will not sufficiently correct the dense cloud. Thus, the decision to include or exclude manual GCPs should be decided on a case-by-case basis to ensure the construction of high-quality products from which scientific information can be extracted via topographic differencing, morphometric mapping, or topographic analysis. However, while ICP alignment proves useful and time efficient,

may only be applicable to landscapes that have not experienced significant topographic or vegetative change. This is due to the technique's reliance on point similarity between the reference point cloud and the QUAKES-I point cloud.

Quality of Topographic Products

The QUAKES-I topographic produced with our photogrammetric pipeline are high quality and show promise for use in active tectonics and geomorphological studies, especially where other high-quality data are not available, and for event response. Our quality assessments using Cloud Compare software show that QUAKES-I dense clouds are comparable to 3DEP and EarthScope lidar datasets in terms of accurately visualizing topography at the 1.5-to-2-meter resolution. After ICP alignment, offsets between the QUAKES-I data and reference lidar were minimal and consistent with the difference in raster resolution (0.5 and 1 meters compared to 1.5-1.6 meters). The trade-off of higher resolution with lidar for acquisition speed and area of coverage with stereo-imaging is justifiable for rapid response reconnaissance (e.g. earthquakes, landslides, fires) and analysis of geological features such as faults where the optimal mapping resolution is 0.5 to 5 meters. Further comparison of QUAKES-I DEMs and DTMs with lidar-derived products will provide better insight into the differences in data quality for the two approaches.

Next steps

Our next steps include refining the processing pipeline and generating more products from 2021 and 2022 QUAKES-I surveys for scientific study.

- Test the utility of applying an image-sharpening algorithm in place of the grey-scale conversion in the pre-processing stage to extract points from areas distorted by shadows.
- Experiment with parameters in constructing the color ortho-mosaics to minimize artifacts and color distortion.
- Compare the QUAKES-I products' quality between surveys and to alternative datasets with cloud-to-cloud distance measurements, DEM/DTM differencing, and spectral analysis of the color ortho-mosaics.
- Extract scientific information from the QUAKES-I topographic products.
- This includes fault trace delineation (mapping), land surface reconstruction of fault zones (measuring fault offsets, slip per event, and slip rates), and quantifying the land surface response to tectonic and geomorphic deformation.
- To extract this information, we will compute topographic metrics (e.g., slope, curvature, geomorphons) from QUAKES-I DEMs to map fault traces, geomorphic features, and surficial geological units.

- We will use morphologic dating and topographic measuring algorithms to extract fault offsets as well as the morphologic ages of scarps and the surfaces they crosscut.
- We will leverage topographic differencing to test the utility of QUAKES-I products for rapid response and quantify surface change post-earthquake and post-mass movement events.

Summary

- We developed a reproducible photogrammetric processing pipeline using open-source Python libraries, Agisoft Metashape Professional Edition 1.8.4, and Cloud Compare to successfully process QUAKES-I imagery.
- Initial topographic products for the Panamint Valley and the San Andreas Fault creeping section generated with Metashape exhibit systematic ~380-meter horizontal offset ~20 degrees from the flight path (prior to geolocation correction with GCPs or ICP alignment).
- After performing geolocation correction, topographic products for the Panamint Valley and the San Andreas Fault creeping section yield DEM/DTM resolutions of 1.5-1.6 meters/pixel and classifiable point clouds demonstrating <5-8-meter accuracy.
- The total end-to-end processing times (including pre-processing, SfM, manual GCP correction, and quality assessment in Cloud Compare) are 5 hours and 3 minutes for the Panamint Valley chunk and 6 hours and 2 minutes for the SAF creeping section chunk.
- With Metashape software, camera position/orientations are necessary to properly reconstruct topography with SfM. Additional geolocation corrections with GCPs and ICP alignment are necessary to correct warp (present in the Panamint Valley model) and systematic horizontal offset (present in all models).

Code

https://github.com/madelineschwarz/QUAKES-photogrammetry

References

Agisoft LLC. (2022). Agisoft Metashape Professional Edition 1.8 User Manual. https://www.agisoft.com/pdf/metashape-pro_1_8_en.pdf

Betlem, P., & Rodes, N. (2022). Geo-SfM - Geo-Structure-from-Motion Course: v2022.09.07 (v2022.09.07). Zenodo. https://doi.org/10.5281/zenodo.7057605

Claverie, M., Ju, J., Masek, J. G., Dungan, J. L., Vermote, E. F., Roger, J. C., Skakun, S. V., & Justice, C. (2018). The Harmonized Landsat and Sentinel-2 Surface Reflectance Data Set. Remote Sensing of Environment, 219, 145-161.

EarthScope Southern & Eastern California LiDAR Project (2009). Distributed by OpenTopography. https://doi.org/10.5069/G9G44N6Q . Accessed: 2023-9-26.

EOX IT. (2021). Sentinel-2 Cloudless. https://s2maps.eu

Jayko, A.S., 2009, Surficial geologic map of the Darwin Hills 30' x 60' quadrangle, Inyo County, California: U.S. Geological Survey Scientific Investigations Map 3040, 20 p. pamphlet, 2 plates, scale 1:100,000.

Johnson, K., Nissen, E., Saripalli, S., Arrowsmith, J.R., McGarey, P., Scharer, K., Williams, P., Blisniuk, K., 2014, Rapid mapping of ultrafine fault zone topography with structure from motion. *Geosphere* ;; 10 (5): 969–986. doi: https://doi.org/10.1130/GES01017.1

U.S. Geological Survey (2018). CA FEMA Z4 B1 2018. Distributed by OpenTopography. https://portal.opentopography.org/usgsDataset?dsid=CA_FEMA_Z4_B1_2018, last accessed 2023-10-11.

U.S. Geological Survey, 2020, Quaternary Fault and Fold Database for the Nation, accessed October 25, 2023, at https://doi.org/10.5066/P9BCVRCK